Supplementary Information

Sulfonated NbS_2-based proton-exchange membrane for vanadium redox flow batteries

Hossein Beydaghi,[a,b&] Sebastiano Bellani,[b&] Leyla Najafi,[b] Reinier Oropesa-Nuñez,[c] Gabriele Bianca,[a,d] Ahmad Bagheri,[a] Irene Conticello,[b] Beatriz Martín-García,[a] Sepideh Kashefi,[e] Michele Serri,[a] Liping Liao,[f] Zdeněk Sofer,[f] Vittorio Pellegrini,[a,b] and Francesco Bonaccorso[a,b,*]

[a] *Graphene Labs, Istituto Italiano di Tecnologia, via Morego 30, 16163 Genoa, Italy*

[b] *BeDimensional SpA, via Lungotorrente Secca 30R, 16163 Genoa, Italy*

[c] *Department of Material Science and Engineering, Uppsala University, Box 534, 75103 Uppsala, Sweden*

[d] *Dipartimento di Chimica e Chimica Industriale, Università degli Studi di Genova, via Dodecaneso 31, 16146 Genoa, Italy*

[e] *Department of Chemical Engineering, Semnan University, Semnan, 3513119111, Iran*

[f] *Department of Inorganic Chemistry, University of Chemistry and Technology Prague, Technická 5, 166 28 Prague 6, Czech Republic*

& These authors contributed equally

S.1 Experimental

* Corresponding author: E-mail address: Francesco.Bonaccorso@iit.it (Francesco Bonaccorso).

S.1.1. Materials

Poly (ether ether ketone) (PEEK) powder (Mw: 28800 g mol^{-1}), sodium 3-mercapto-1-propane sulfonate salt (SMPS) (90%), dimethyl sulfoxide (DMSO) (≥ 99.9%), anhydrous isopropyl alcohol (IPA) (exfoliating solvent for NbS_2 crystals), concentrated sulfuric acid (H_2SO_4, 95–98%) (sulfonation agent) and 1-methyl-2-pyrrolidone (NMP) (solvents for PEEK, sulfonated PEEK (SPEEK) and sulfonated nibium disolfide (S-NbS_2)) were purchased from Sigma Aldrich. Niobium (Nb, 99.9 %, <100 μm) and Sulphur (S, 99.999 %, < 6mm) powder were purchased from Strem Chemicals, Inc. Vanadium (IV) sulfate oxide ($VOSO_4$) (99.9%, metals basis) was purchased from Alfa Aesar. All chemicals were used as received without any further purification.

S.1.2. Synthesis of NbS_2 and S-NbS_2 nanoflakes

The crystals of NbS_2 were produced in form of *2H*/*3R* phase mixture by direct synthesis from their composing elements (*i.e.*, Nb and S), following previous protocols.[1,2] An appropriate amount of Nb and S powders (Nb:S stoichiometry = 1:2) corresponding to 10 g of NbS_2 were placed into a quartz glass ampoule (20 mm×120 mm) and sealed under high vacuum (1×10^{-3} Pa). After reaching vacuum, the ampoule was heated at 450 °C for 12 h and subsequently at 600 °C for 48 h. Afterward, the resulting materials were treated at 900 °C for 48 h and cooled down to room temperature over a period of 24 h to obtain the NbS_2 crystals. The heating/cooling rate was ±5 °C min^{-1} for all the heating/cooling steps. The NbS_2 nanoflakes were produced in form of dispersion in IPA through liquid-phase exfoliation (LPE) of the NbS_2 crystals,[3,4] followed by sedimentation-based separation.[5,6] Experimentally, 50 mg of the produced NbS_2 crystals were dispersed in 500 mL of IPA and then ultrasonicated (Branson® 5800 cleaner, Branson Ultrasonics) for 6 h. Subsequently, the resulting dispersion was ultracentrifuged (Optima™ XE-90 with a SW32Ti rotor, Beckman Coulter) at 2700 *g* for 20 min at 15 °C to separate the exfoliated materials remained in the supernatant from un-exfoliated bulk crystals. After the ultracentrifugation process, 80% of the supernatant was collected by pipetting, thus obtaining a dispersion of NbS_2 nanoflakes with a concentration of 0.86 g L^{-1}.

The LPE-produced NbS_2 nanoflakes were chemically functionalized using SMPS salt.[1] Briefly, the NbS_2 nanoflakes dispersion in IPA (10 mg mL^{-1}) (20 mL) was heated at 70 °C for 5 h under vigorous magnetic stirring in presence of SMPS (820 mg) dispersed in 20 mL of DMSO. The unreacted SMPS was removed by means of a washing procedure combining centrifugation and solvents. First, the material was recovered by centrifugation (Sigma 3-16P centrifuge, rotor 19776)

for 10 min at 2599 *g*. Then, the material was washed four times using a mixture of IPA:DMSO (1.5:1 vol:vol) and once more only with IPA to remove the residual DMSO, by combining redispersion using ultrasonication in a sonic bath for 5 min with ultracentrifugation (Sigma 3-16P centrifuge, rotor 19776) for 10 min at 2599 *g* to recover the material. After the washing process, the SMPS-functionalized NbS_2 (hereafter named S-NbS_2) nanoflakes were redispersed in NMP by ultrasonication for 20 min to obtain the final ink concentration of 18 mg mL^{-1}.

S.1.3. Sulfonation of polymer

The SPEEK was prepared following the protocols reported in our previous works.[7] Various degree of sulfonation (DS) of polymers were investigated, finding an optimum DS of 70.2 %.[1] Experimentally, 1 g of PEEK was dried overnight at 60 °C and then slowly dissolved in concentrated H_2SO_4 under vigorously stirring. The sulfonation reaction was performed at 25 °C for 1 h and then 60 °C for 5 h and 20 min. Afterwards, the solution was cooled down to room temperature. The final solution was added to the large excess of iced cold water under continuous stirring. The obtained white precipitate was washed with deionized water until reaching a neutral pH to remove residual acid, followed by drying at 70 °C under vacuum overnight. The DS of as-produced SPEEK was measured to be 70.2 % by acid-base titration method.

S.1.4. Membrane preparation

The SPEEK and SPEEK/S-NbS_2 membranes were prepared *via* solution casting method using NMP solvent. In a previous study from the authors,[8] the effect of solvent on the properties of the resulting SPEEK-based membranes was investigated, indicating that the membranes casted using NMP exhibited higher proton conductivity (σ), higher water uptake and more compact morphology compared to those obtained using DMSO or N,N-dimethyl acetamide (DMAc) solvents. Hereafter, the as-produced membranes are named SPEEK and SPEEK:x% S-NbS_2, respectively, in which x is the weight percentage of the S-NbS_2 nanoflakes. Experimentally, the SPEEK solution was prepared *via* dissolving appropriate amount of SPEEK into NMP (1/10 wt/vol) and magnetically stirring at 60 °C for 2 h. Afterwards, S-NbS_2 nanoflakes dispersed in NMP were added to the parts of SPEEK solution according to the required wt% of additive (between 1.5-3 wt%). The as-obtained mixtures were stirred for 4 h at 60 ºC, and then cooled down to room temperature. The membranes were obtained by casting the polymeric mixture onto a glass plate by the doctor blade and drying at 80 ºC for 12 h, 120 ºC for 12 h, and 140 ºC for 4 h in vacuum oven. The pristine SPEEK membrane was prepared using the same procedure without using S-NbS_2 nanoflakes as

the additives. After drying, the average thickness of the produced membranes ranged from 100 to 130 μm. The membranes were activated with 1 M H_2SO_4 for 12 h at room temperature before the experiments.[9]

S.1.5. Characterization of materials and membranes

Bright-field transmission electron microscopy (BF-TEM) images were taken using a JEM 1011 (JEOL) TEM (thermionic W filament), working with an acceleration voltage of 100 kV. The samples were prepared by drop casting nanoflakes dispersions onto ultrathin C-film on holey carbon 400 mesh Cu grids (Ted Pella Inc), subsequently washed with deionized water and dried at room temperature in vacuum overnight. Morphological and statistical analyses of the lateral dimension of the S-NbS_2 nanoflakes were performed using ImageJ software (NIH) and OriginPro 9.1 software (OriginLab), respectively. X-ray diffraction (XRD) patterns of the NbS_2 and S-NbS_2 nanoflakes were recorded using the PANalytical Empyrean X-ray diffractometer with Cu Kα radiation. Raman spectra were recorded using a Renishaw microRaman Invia 1000 spectrometer and a laser wavelength of 532 nm. The as-prepared dispersions were drop-cast onto Si/SiO_2 substrates and dried under vacuum overnight for XRD and Raman analyses. Fourier-transform infrared (FTIR) spectra of the produced nanoflakes were recorded using a single-reflection ATR accessory (MIRacle ATR, Pike Technologies) coupled to a FTIR spectrometer (Equinox 70 FT-IR, Bruker) in the wavelength range from 2000 to 600 cm^{-1}, with a resolution of 4 cm^{-1} and accumulating 128 scans.

The nanoflakes thickness was measured using a Bruker Dimension Icon atomic force microscope (AFM, Bruker Dimension Icon, Billerica, MA, USA). The measurements were carried out in intermittent contact mode using RTESPA cantilevers (Bruker, Billerica, MA, USA) with a tip with a nominal diameter of 8 nm. A drive frequency of ~300 kHz was used for the image acquisition. The images were collected over an area of 2.5×2.5 μm^2 (512×512 data points) and using a scan rate of 0.7 Hz. The height profile analysis was performed using Gwyddion 2.54 software. The AFM data were analyzed using OriginPro 9.1 software. The samples were fabricated by depositing the nanoflake dispersions onto mica substrates (G250-1, Agar Scientific Ltd.). The samples were dried under vacuum overnight before being measured.

The morphology of the produced membranes was evaluated by scanning electron microscopy (SEM) using a JEOL JSM-6490LA SEM Analytical (low-vacuum) microscope. The membranes were prepared by freeze-fracturing in liquid nitrogen, followed by coating with a thin layer of gold.

The distribution of Nb in the samples was assessed by energy dispersive X-ray spectroscopy (EDX) measurements. The thermal stability of the prepared membranes was investigated by thermogravimetric analysis (TGA), using TGA Q500 (TA Instruments, USA) thermogravimetric analyzer. The TGA tests were performed in nitrogen atmosphere in a 25–800 °C temperature range and using a heating rate of 10 °C min^{-1}. The mechanical properties of the produced membranes were assessed using the STM-50 testing machine (SANTAM, Iran), with an operating rate of 2 mm min^{-1} at room temperature.

Adhesion force/work measurements of the membranes were carried out using a Bruker Dimension Icon atomic force microscope (Bruker Dimension Icon, Billerica, MA, USA). Force volume measurements were acquired using V-shaped DNP silicon nitride cantilevers (Bruker, Billerica, MA, USA), with a nominal spring constant of 0.06 N m^{-1}, resonance frequency in air in the 40–70 kHz range and tip typical curvature radius of 20–60 nm. The actual spring constant of each cantilever was determined in situ, using the thermal noise method. The acquisition of a large set of force–distance (FD) curves (4096 curves) was performed in humid ambient air (relative humidity –RH– ~75%) with a maximum force load of 20 nN and a curve length of 800 nm per each sample. Adhesion force maps of 10 × 10 μm^2 images were collected. The adhesion work data were analyzed with OriginPro 9.1 software.

The ion exchange capacity (IEC) of the produced PEMs was measured using the conventional acid-base titration method. Dried membranes were immersed into a 50 mL saturated NaCl solution for 2 days in order to exchange the H^+ with Na^+, followed by titration with 0.01 mol L^{-1} NaOH solution, using phenolphthalein as an indicator. The IEC value of the PEMs was calculated according to the equation:

$$IEC = \frac{V_{NaOH} \times C_{NaOH}}{W_{dry}}$$

where, V_{NaOH} is the volume of the NaOH solution consumed in the titration, C_{NaOH} is the concentration of the used NaOH solution and W_{dry} is the weight of the dry membrane.

The water uptake (WU) and membrane swelling (MS) of the prepared membrane were measured by the membrane change on weights and dimensions in dry and wet conditions at different temperature. The weighed dry membranes were immersed, after the measurement of their area dimension, in the deionized water for 12 h, then taken out and put between two clean filter papers

to remove residual water and finally weighed and measured. The WU and MS values of the prepared membranes were calculated according to the following equations:

$$\mathrm{WU}\,(\%) = \frac{W_w - W_d}{W_d} \times 100$$

in which, W_w is the weight of the wet membrane, and W_d is the weight of the dry membranes;

$$\mathrm{MS}\,(\%) = \frac{A_w - A_d}{A_d} \times 100$$

in which, A_w is the membrane area after 12 h soaking in deionized water, and A_d is the area of the dry membrane.

The chemical stability of the membranes was tested by soaking the samples in 1.5 M VO_2^+ + 3 M H_2SO_4 solutions, kept at room temperature for 30 days. The membrane weight loss after 30 days was calculated by:

$$\text{Weight loss} = \frac{W_0 - W}{W_0}$$

in which, W_0 and W are the initial and final membrane weight, respectively.

The σ (S cm^{-1}) of the prepared membranes was calculated by measuring the membrane resistance (R), (Ω) through electrochemical impedance spectroscopy (EIS). The EIS tests were performed with a potentiostat/galvanostat (VMP3, Biologic) using two platinum electrodes, over a frequency range of 2 mHz-100 kHz with oscillating voltage amplitude of 50 mV. Before the electrochemical tests, the membranes were fully humidified by immersion in deionized water. The σ of the membranes was calculated by:

$$\sigma = \frac{L}{R.A}$$

In which L is the thickness of the membrane (cm), and A is the electrode area in contact with the membrane (cm^2).

The vanadium ion permeability (P) of the produced membranes were measured by using home-made diffusion cell, *i.e.*, a cell is composed of two different compartments separated by the membrane under study. One of the cell compartments was filled with 25 mL of 1 M $VOSO_4$ in 3

M H_2SO_4 solution, and an equal volume of 1 M $MgSO_4$ in 3 M H_2SO_4 solution was added to the second cell compartment to minimizes the osmotic pressure between the two solutions. Magnetic stirring bar was used in both compartments to mix the solutions and avoid concentration polarizations. The concentration of VO^{2+} in the second cell compartment was periodically measured using a UV-vis spectrometer (UT-1800, China) at 760 nm. Then, the P of the membranes was calculated according to the following equation:

$$C_B(t) = \frac{AP}{LV_B} C_A(t - t_0)$$

In which C_A and C_B (mol L^{-1}) are the VO^{2+} concentrations in first and second cell compartments, respectively, A (cm^2), L (cm) are the effective area and thickness of membrane, respectively, V_B (cm^3) is the solution volume in the second cell compartment, and t is the time.

The selectivity (S min^{-1} cm^{-3}), was used as an important indicator to investigate the overall VRFB's PEM properties: and calculated by:

$$\text{Selectivity} = \frac{\sigma}{P}$$

The vanadium redux flow batteries (VRFBs) were assembled using a no-gap serpentine architecture (XLScribner RFB Single Cell Hardware). This hardware assembly consists of pairs of: Poco Graphite flow-field layout-based graphite bipolar plates (Poco®), Teflon® flow frames, Viton® rubber gaskets and Au-plated Al end plates with electrolyte input/output ports (Swagelok® fittings). The as-prepared SPEEK and SPEEK:S-NbS_2 membranes were used as PEMs. Nafion 115 was also investigated as PEM for benchamarking purposes. Peristaltic pumps (Masterflex L/S® Series) were used to flow the electrolyte into the cell hardware. Functionalized graphite felts with a thickness of 4.6 mm and an area of 2×2 cm were used as electrodes. According to our previous work [10], graphite felts were treated by combined multiple gas plasma, namely O_2:N_2 plasma with a 1:1 wt/wt composition, in an inductively coupled radio frequency (13.56 MHz) reactor at a power of 100 W and a process pressure of 16 Pa (background gas pressure of 0.2 Pa) for 10 min.

The electrochemical measurements of the VRFBs were performed with a potentiostat/galvanostat (VMP3, Biologic, France). The VRFBs were evaluated using 1 M VO^{2+} + 3 M H_2SO_4 and 1 M V^{3+} + 3 M H_2SO_4 as the starting catholyte and anolyte, respectively. The electrolytes were prepared

from 1 M $VOSO_4$ + 3 M H_2SO_4 solution by electrochemical method.[11] The electrolytes were pumped with a flow rate of 30 mL min^{-1}. Nitrogen was purged into the negative electrode reservoirs (containing V^{2+} and V^{3+}) to avoid oxidation of V^{2+} during the charged state of the batteries. The polarization curve analysis was performed on charged VRFBs. The charged state of the VRFBs was reached by applying a constant current density of 100 mA cm^{-2} and an upper voltage limit of 1.8 V. The VRFBs were then discharged for 30 s at each applied current density (ranging from 1 to 920 mA cm^{-2}). Cell voltage measurements were averaged over the 30 s of each current step to provide a point of the polarization curve. Before acquiring the polarization curves, the high-frequency resistance of the VRFB was measured by EIS at 30 kHz, in agreement with previous protocols.[12] The amplitude of the AC voltage perturbation was 10 mV. The iR-losses were calculated by the product between the applied current (i) and the high-frequency resistance measured by EIS. The iR-corrected polarization curves were obtained by subtracting the iR-losses to the raw polarization curves. The galvanostatic CD measurements of the VRFBs were carried out at different current densities (ranging from 25 to 400 mA cm^{-2}). The lower and upper cell voltage limits were set to 1 and 1.6 V, respectively to avoid parasitic reactions, following recommended practices.[13] Self-discharge measurements were carried out measuring the open circuit voltage of the VRFBs (area = 20 cm^2) over time, starting from a 90% state-of-charge.

S.2. ATR-FTIR characterization of the NbS_2 and S-NbS_2 nanoflakes

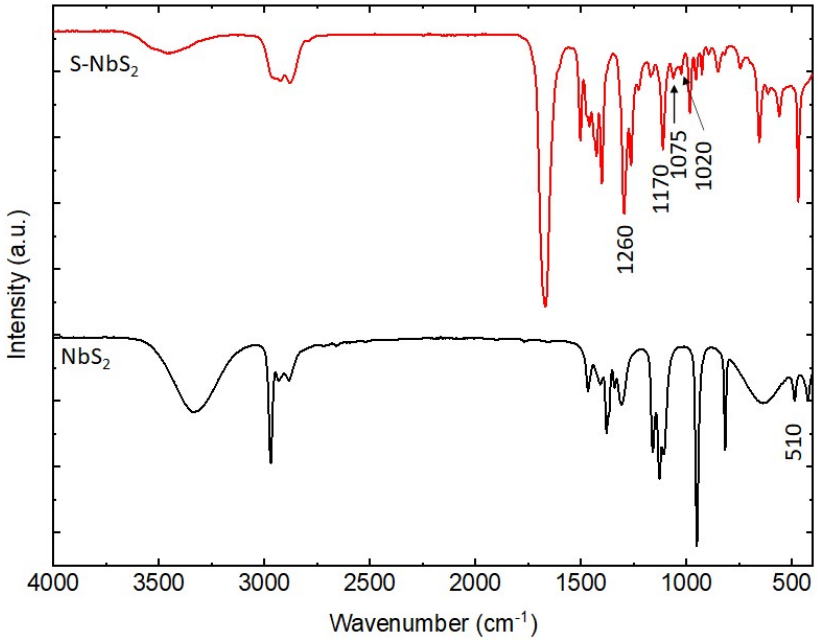

Fig. S1 *ATR-FTIR spectra of the NbS_2 and S-NbS_2 nanoflakes.*

Fig. S1 shows the ATR-FTIR spectra of the NbS_2 and S-NbS_2 nanoflakes. In the ATR-FTIR spectrum of the NbS_2 nanoflakes, the observed peak at ~500 cm^{-1} is assigned to the Nb–S stretching vibration. In the S-NbS_2 nanoflakes, the strong characteristic peaks at 1020, 1075, and 1260 cm^{-1} are associated to the asymmetric and symmetric stretching vibration of O=S=O and the stretching vibration of S=O, respectively.[14] In addition, the observed absorption peak at ~1170 cm^{-1} indicates the presence of SMPS in the S-NbS_2 nanoflakes.[15] The peaks at 2850 and 2920 cm^{-1} are due to the asymmetrical stretching vibration of CH_2.[16] The difference in the shape and intensity of asymmetric and symmetric Nb-S peak in the S-NbS_2 is due to increasing number of the Nb-S bonds with reaction between NbS_2 nanoflakes and SMPS (see Scheme 1 in the main text). The observed sharp peak at ~1700 cm^{-1} in the ATR-FTIR of the S-NbS_2 nanoflakes is probable related to the residual presence of NMP, which is used as the processing solvent of S-NbS_2.

S.3. Supplementary membrane characterization

Table S1. *Membrane parameter (thickness, IEC, tensile stress and elongation at break (E_b)) values measured for the investigated membranes at room temperature.*

membrane	Thickness (µm)	IEC (meq. g^{-1})	Tensile stress (MPa)	E_b (%)
SPEEK	116	1.68	32.4	12.8
SPEEK:1.5% S-NbS_2	112	1.81	35.9	12.1
SPEEK:2.0% S-NbS_2	106	1.94	36.5	11.9
SPEEK:2.5% S-NbS_2	103	2.02	36.9	11.8
SPEEK:3.0% S-NbS_2	102	2.10	37.1	11.7

Generally, the IEC relies on the water absorption capability and reflects the proton exchangeable groups density (–SO_3H group value) of membranes. Similar to the membrane WU, membrane σ increases with increasing IEC. Table S1 presents the IEC of the pristine SPEEK and nanocomposite membranes. Compared to the SPEEK membrane (IEC = 1.68 meq. g^{-1}), the nanocomposite membranes show higher IECs, indicating an increase of the proton exchangeable groups in the polymeric chains of SPEEK. In fact, the proton-conducting groups of the S-NbS_2 nanoflakes increase the IECs of the corresponding nanocomposite membranes over those of the pristine SPEEK due to the high -SO_3H content of the S-NbS_2 nanoflakes. The increase of the IEC decreases the distance between ion exchangeable groups, accelerating the proton transfer through the membrane.

Since the electrolyte passes across the membrane, the mechanical strength of the used membrane has an important role in determing the long-term stability of a membrane during VRFB operation. The stress–strain behaviour of the produced membranes was evaluated in dry condition. As shown in Table S1, the nanocomposite membranes exhibit tensile strength in the 35.9–37.1 MPa range. These values are higher than that of the pristine SPEEK membrane (32.4 MPa). With increasing the S-NbS_2 content to 3 wt%, the tensile strength of the nanocomposite membrane reached the maximum value of 37.1 MPa. The incorporation of the S-NbS_2 nanoflakes into the polymeric

matrix can enhance the mechanical strength of the nanocomposite membrane owing to strong hydrogen bonding interactions between the sulfonated groups of the S-NbS_2 and SPEEK.[17] Moreover, the E_b of the produced membranes, ranging from 11.7% to 12.8%, decreases with increasing the content of S-NbS_2 nanoflakes because of formation of strong hydrogen bonding with SPEEK chains, which densify the membrane structure while limiting the polymer chains mobility.

S.4. TGA analysis

A TGA analysis was performed in nitrogen atmosphere to analyze the thermal properties of the produced membranes. **Fig. S2** shows the TGA curves recorded for pristine SPEEK and SPEEK:2.5% S-NbS_2 nanocomposite membranes. The SPEEK and SPEEK:2.5% S-NbS_2 decomposition processes show similar trends consisting of three steps: (i), around 100 °C, associated to the elimination of the residual water and solvent,[18] (ii), around 250 °C, related to the decomposition of the sulfonic groups (SO^{3-}),[19] and (iii), around 500 °C, associated to the polymer main chain degradation.[20] Meanwhile, the amount of S-NbS_2 nanoflakes in the SPEEK:2.5% S-NbS_2 nanocomposite membranes can be further confirmed by TGA data, since they are stable up to 800°C without any weight loss.[21] According to the measured weight losses, the S-NbS_2 nanoflakes amount in the SPEEK:2.5% S-NbS_2 membrane is 2.4 %, which resembles the expected value of 2.5% used for the synthesis process. In addition, our TGA results suggest that the various produced membranes meet the thermal properties requirement of PEMs applied in VRFBs, which typically work at temperatures lower than 100 °C under oxygen-free atmosphere.

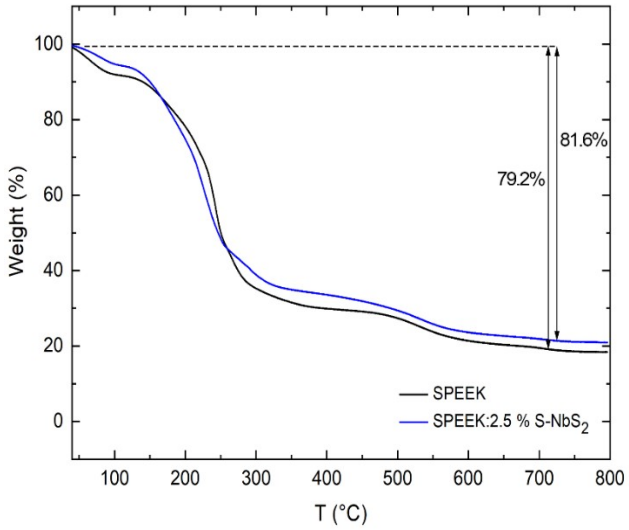

Fig. S2 *TGA curves of the SPEEK and SPEEK:2.5% S-NbS_2 membrane.*

S.5. Comparison of membranes

Table S2. *Comparison between CE, VE and EE of our SPEEK:2.5% S-NbS_2 membrane with those of membranes reported in literature.*

Membranes	Current density (mA cm^{-2})	CE (%)	VE (%)	EE (%)	Ref.
SPEEK:2.5% S-NbS_2	100	98.8	90.2	89.3	This work
	200	99.2	81.1	80.1	
	300	99.5	73.2	72.8	
Nafion 115	100	98.0	86.9	85.2	This work
SPEEK/ZC-GO[a]	100	99.0	85.8	81.8	17
SPEEK/GO-BDSA[b]	100	97.8	82.0	79.0	22
SPEEK/PBI[c]	100	98.7	86.0	85.0	23
SPEEK/PBI	100	98.6	89.0	88.0	24
SPEEK/ImPPO[d]	100	98.0	80.0	81.0	25
SPEEK/TiO_2	100	97.6	71	69	26
SPEEK/PTFE[e]	100	98.5	79.5	79.0	27
SPEEK/PTFE	200	99.3	65.0	64.9	28
SPEEK/PAN[f]	200	97.2	70.9	69.6	29
SPEEK/PPO-TTA[g]	200	98.3	79.8	77.11	30
SPEEK/PDA[h]	200	98.5	67.5	66.5	31
SPEEK/GO[i]	200	98.4	71.5	70.5	32
SPEEK/PES[j]	200	99.1	79.0	78.0	33
SPEEK/DHNT[k]	200	98.4	78.0	77.5	34
SPEEK/ImPSf[l]	200	97.5	80.5	77.3	35
SPEEK/lignin	300	99.3	57.0	56.5	36
SPEEK/Nafion/h-BN[m]	100	97.2	88.0	86.5	37
Nafion 212	100	86.5	90.8	78.9	30
Nafion 212	200	92.0	77.5	72.0	34
Nafion 115	100	94.5	86.0	82.0	23
Nafion 115	100	95.0	87.0	86.0	38

Nafion 115	200	95.8	77.0	74.0	[39]
Nafion 117	100	96.8	76.8	74.7	[17]
Nafion 117	100	96.9	77.0	75.0	[40]
Nafion 117	200	95.0	66.9	63.8	[28]

a. zwitterion-decorated graphene oxide, b. 2,2′-benzidinedisulfonic acid-functionalized amphoteric graphene oxide, c. polybenzimidazole, d. imidazolium-functionalized polyphenylene oxide, e. porous poly(tetrafluoroethylene), f. polyacrylonitrile, g. triple tertiary amine-grafted poly(2,6-dimethyl-1,4-phenylene oxide), h. polydopamine, i. graphene oxide, j. poly(ether sulfone), k. dopamine-modified halloysite nanotubes l. imidazolium-functionalized polysulfone m. hexagonal boron nitride

S.6. Self-discahrge measurements

Self-discahrge measurements were carried out on the most performant VRFB, namely, SPEEK:2.5% S-NbS_2, comparing the results with those recorded for a reference cell based on Nafion 115. As shown in Fig. S3, the discharge time of SPEEK:2.5% S-NbS_2 was higher (~+102%) than the one of Nafion 115-based VRFBs, indicating the lower vanadium ion permeability of the nanocomposite membrane if compared with Nafion 115.

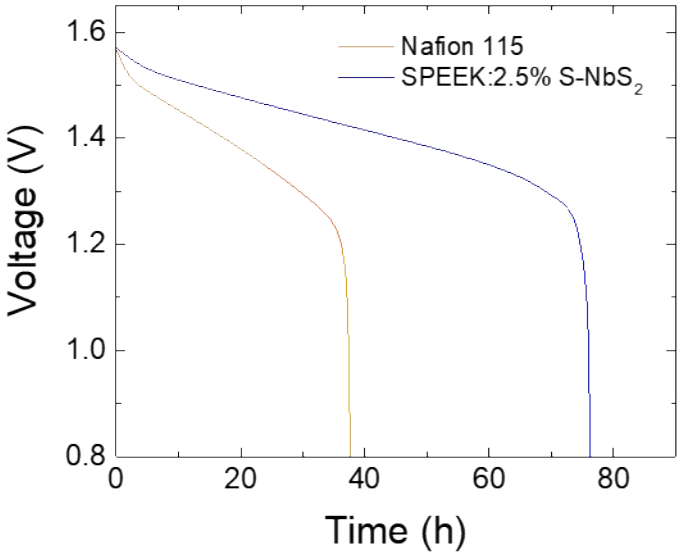

Fig. S3 *Open circuit voltage of SPEEK:2.5% S-NbS_2 and Nafion 115-based VRFB as a function of time, starting from a 90% state-of-charge.*

References

1 L. Najafi, S. Bellani, R. Oropesa-Nuñez, B. Martín-García, M. Prato, V. Mazánek, D. Debellis, S. Lauciello, R. Brescia, Z. Sofer and F. Bonaccorso, *J. Mater. Chem. A*, 2019, **7**, 25593–25608.

2 L. Najafi, S. Bellani, R. Oropesa-Nuñez, B. Martín-García, M. Prato, L. Pasquale, J.-K. Panda, P. Marvan, Z. Sofer and F. Bonaccorso, *ACS Catal.*, 2020, **10**, 3313–3325.

3 V. Nicolosi, M. Chhowalla, M. G. Kanatzidis, M. S. Strano and J. N. Coleman, *Science, 2013, **340,** 6139.*

4 F. Bonaccorso, A. Bartolotta, J. N. Coleman and C. Backes, *Adv. Mater.*, 2016, **28**, 6136–6166.

5 O. M. Maragó, F. Bonaccorso, R. Saija, G. Privitera, P. G. Gucciardi, M. A. Iatì, G. Calogero, P. H. Jones, F. Borghese, P. Denti, V. Nicolosi and A. C. Ferrari, *ACS Nano*, 2010, **4**, 7515–7523.

6 A. Capasso, A. E. Del Rio Castillo, H. Sun, A. Ansaldo, V. Pellegrini and F. Bonaccorso, *Solid State Commun.*, 2015, **224**, 53–63.

7 A. A. Zadeh, H. Mazdarani, H. Beydaghi, E. Tabrizian and M. Javanbakht, US Patent, 2020, 16,109,347.

8 A. Bagheri, M. Javanbakht, H. Beydaghi, P. Salarizadeh, A. Shabanikia and H. Salar Amoli, *RSC Adv.*, 2016, **6**, 39500–39510.

9 P. Salarizadeh, A. Bagheri, H. Beydaghi and K. Hooshyari, *Int. J. Energy Res.*, 2019, **43,** 4048–4853.

10 S. Bellani, L. Najafi, M. Prato, R. Oropesa-Nuñez, B. Martín-García, L. Gagliani, E. Mantero, L. Marasco, G. Bianca, M. I. Zappia, C. Demirci, S. Olivotto, G. Mariucci, V. Pellegrini, M. Schiavetti and F. Bonaccorso, *Chem. Mater.*, 2021, **33**, 4106–4121.

11 W. Li, R. Zaffou, C. C. Sholvin, M. L. Perry and Y. She, *ECS Trans.*, 2013, **53,** 93.

12 D. Aaron, Z. Tang, A. B. Papandrew and T. A. Zawodzinski, *J. Appl. Electrochem.*, 2011, **41**, 1175.

13 L. Wu, J. Wang, Y. Shen, L. Liu and J. Xi, *Phys. Chem. Chem. Phys.*, 2017, **19,** 14708–14717.

14 T. Y. Inan, H. Doğan, E. E. Unveren and E. Eker, *Int. J. Hydrogen Energy*, 2010, **35**, 12038–12053.

15 https://pubchem.ncbi.nlm.nih.gov/compound/Sodium-3.

16 W. Li, X. Wei, H. Dong, Y. Ou, S. Xiao, Y. Yang, P. Xiao and Y. Zhang, *Front. Chem.*, 2020, **8,** 189.

17 Y. Zhang, H. Wang, B. Liu, J. Shi, J. Zhang and H. Shi, *J. Mater. Chem. A*, 2019, **7**, 12669–12680.

18 X. Liu, Y. Zhang, S. Deng, C. Li, J. Dong, J. Wang, Z. Yang, D. Wang and H. Cheng, *ACS Appl. Energy Mater.*, 2018, **1**, 5463–5473.

19 D. Marani, A. D'Epifanio, E. Traversa, M. Miyayama and S. Licoccia, *Chem. Mater.*, 2010, **22**, 1126–1133.

20 T. Yang, Z. Li, H. Lyu, J. Zheng, J. Liu, F. Liu, Z. Zhang and H. Rao, *RSC Adv.*, 2018, **8**, 15740–15753.

21 Z. Xiao, Z. Yang, L. Zhang, H. Pan and R. Wang, *ACS Nano*, 2017, **11**, 8488–8498.

22 B. Liu, Y. Jiang, H. Wang, J. Ge and H. Shi, *Energy & Fuels*, 2020, **34**, 2452–2461.

23 L. Qiao, H. Zhang, M. Li, Z. Yuan, Y. Zhao and X. Li, *J. Mater. Chem. A*, 2017, **5**, 25555–25561.

24 D. Chen, X. Chen, L. Ding and X. Li, *J. Memb. Sci.*, 2018, **553**, 25–31.

25 F. Chu, X. Chu, T. Lv, Z. Chen, Y. Ren, S. Zhang, N. Yuan, B. Lin and J. Ding, *ChemElectroChem*, 2019, **6**, 5041–5050.

26 Y. Ji, Z. Y. Tay and S. F. Y. Li, *J. Memb. Sci.*, 2017, **539**, 197–205.

27 J. Kim, Y. Lee, J.-D. Jeon and S.-Y. Kwak, *J. Power Sources*, 2018, **383**, 1–9.

28 L. Yu and J. Xi, *ACS Appl. Mater. Interfaces*, 2016, **8**, 23425–23430.

29 Z. Li, W. Dai, L. Yu, L. Liu, J. Xi, X. Qiu and L. Chen, *ACS Appl. Mater. Interfaces*, 2014, **6**, 18885–18893.

30 H. Zhang, X. Yan, L. Gao, L. Hu, X. Ruan, W. Zheng and G. He, *ACS Appl. Mater. Interfaces*, 2019, **11**, 5003–5014.

31 J. Xi, W. Dai and L. Yu, *RSC Adv.*, 2015, **5**, 33400–33406.

32 W. Dai, Y. Shen, Z. Li, L. Yu, J. Xi and X. Qiu, *J. Mater. Chem. A*, 2014, **2**, 12423–12432.

33 W. Lu, Z. Yuan, M. Li, X. Li, H. Zhang and I. Vankelecom, *Adv. Funct. Mater.*, 2017, **27**, 1604587.

34 L. Yu, D. Mu, L. Liu and J. Xi, *J. Memb. Sci.*, 2018, **564**, 237–246.

35 X. Yan, C. Zhang, Y. Dai, W. Zheng, X. Ruan and G. He, *J. Memb. Sci.*, 2017, **544**, 98–107.

36 J. Ye, Y. Cheng, L. Sun, M. Ding, C. Wu, D. Yuan, X. Zhao, C. Xiang and C. Jia, *J. Memb. Sci.*, 2019, **572**, 110–118.

37 J. Liu, L. Yu, X. Cai, U. Khan, Z. Cai, J. Xi, B. Liu and F. Kang, *ACS Nano*, 2019, **13**, 2094–2102.

38 J. Li, Q. Zhang, S. Peng, D. Zhang, X. Yan, X. Wu, X. Gong, Q. Wang and G. He, *J. Memb. Sci.*, 2019, **583**, 93–102.

39 S. Kim, J. Choi, C. Choi, J. Heo, D. W. Kim, J. Y. Lee, Y. T. Hong, H.-T. Jung and H.-T. Kim, *Nano Lett.*, 2018, **18**, 3962–3968.

40 Y. Zhang, H. Wang, W. Yu, J. Shi and H. Shi, *J. Memb. Sci.*, 2018, **564**, 916–925.